Electrochimica Acta 109 (2013) 595–601

Contents lists available at ScienceDirect

Electrochimica Acta

journal homepage: www.elsevier.com/locate/electacta

Low cost, eco-friendly layered $Li_{1.2}(Mn_{0.32}Ni_{0.32}Fe_{0.16})O_2$ nanoparticles for hybrid supercapacitor applications

K. Karthikeyan, S.H. Kim, K.J. Kim, S.N. Lee, Y.S. Lee*

Faculty of Applied Chemical Engineering, Chonnam National University, Gwang-ju 500-757, Republic of Korea

ARTICLE INFO

Article history:
Received 10 April 2013
Received in revised form 25 June 2013
Accepted 14 July 2013
Available online xxx

Keywords:
Layered materials
Hybrid capacitor
Cobalt free
Energy density
Li_2MnO_3

ABSTRACT

$Li_{1.2}(Mn_{0.32}Ni_{0.32}Fe_{0.16})O_2$ (LMNFO) nanoparticles with and without a chelating agent (adipic acid) were synthesized by sol–gel method. The supercapacitive behaviors of the synthesized materials as a cathode are evaluated with activated carbon (AC) as the anode in a hybrid supercapacitor (HSC) configuration utilizing a non-aqueous electrolyte. The structural, morphological and electrochemical features of the prepared materials are investigated using X-ray diffraction, scanning electron microscopy and cyclic voltammetry (CV) and charge–discharge studies, respectively. The results demonstrated that the LMNFO nanoparticles prepared with the chelating agent, adipic acid (AA), delivered an enhanced specific discharge capacitance (86 F g^{-1}) and better cycling stability than the native compound. The CV studies also revealed the same conclusions, based on the stronger current response observed during various scan rates between 0 and 3 V. Moreover, the AA-LMNFO/AC cell delivered maximum energy and power densities of 36 Wh kg^{-1} and 1.67 W kg^{-1}, respectively, with a columbic efficiency of over 99% and excellent rate performance.

1. Introduction

Electrochemical double layer capacitors (EDLC) are expected to bridge the gap between conventional capacitors and secondary batteries and much attention is being paid to the development of such devices due to their high power density, excellent reversibility and durability [1,2]. Currently, EDLCs are being used as the energy storage systems in electronic devices, such as memory backup systems, portable electronic devices, solar panels for energy storage, etc. [3,4]. In the recent past, increasing interest has been paid to the development of the modified version of EDLCs called 'hybrid supercapacitors (HSCs)', because of their higher energy density than that of EDLCs and higher power density than that of rechargeable batteries, for example lithium ion batteries. Thus, it is believed that HSCs can be used to drive electric vehicles (EVs) and hybrid electric vehicles (HEVs) in the near future [5]. Generally, HSCs can be fabricated by coupling a battery-like insertion type electrode with a power source electrode either an EDLC or a pseudo capacitor component. The hybridization of these two kinds of electrodes is a unique approach and is used to enhance the energy and power density of the system in a single device. Carbonaceous materials are the unanimous choice for the EDLC component in the HSC configuration as compared to binary oxides (e.g., RuO_2, IrO_2, Co_3O_4, etc.) and conducting polymers, due to their setbacks such as their cost, long term cycleability, etc. Similarly, the choice of energy source electrode is also very important, because such electrodes should enhance the energy density of the HSC without sacrificing its power density and, hence, several research activities are focused on these intercalating type electrodes [6,7].

Although pre-lithiated graphitic electrode (G) is being utilized for commercialized HSC application along with AC cathode in G/AC configuration, the tedious pre-lithiation process and the formation of solid electrolyte interface during cycling process, hindering the mass production of the graphitic anodes for HSC applications. Therefore, much research is focused to develop transition metal based oxides as insertion type electrodes for HSC applications. So far, various Li-ion intercalating host materials, such as $LiCoO_2$, $LiMn_2O_4$, $LiNi_{1/3}Co_{1/3}Mn_{1/3}O_2$, and $Li_4Mn_5O_{12}$ have been studied as the cathode materials for HSC applications [8–13]. Among the intercalating type energy source electrodes, Mn based materials are appealing, due to their environmentally benignity, natural abundance and cost effectiveness. Spinel $LiMn_2O_4$ has been extensively studied as an electrode material along with either activated carbon (AC) or carbon nanotubes (CNT) in hybrid supercapacitor applications; however, severe capacity fading is encountered during prolonged cycling. In order to overcome the above issue, various transition metal elements are doped in the Mn sites ($LiM_xMn_{2-x}O_4$, M = Ni, Cr, and Co) and this enables better cycling performance to be obtained than that afforded by the native compound, although capacity fading still persists [14,15]. Recently, we reported the use of polyanion type lithium insertion hosts, i.e. Li_2MSiO_4 (M = Fe and Mn) as the electrode material for HSC applications considering

* Corresponding author. Tel.: +82 62 530 1904; fax: +82 62 530 1904.
E-mail address: leeys@chonnam.ac.kr (Y.S. Lee).

0013-4686/$ – see front matter © 2013 Elsevier Ltd. All rights reserved.
http://dx.doi.org/10.1016/j.electacta.2013.07.109

their advantages, such as their cheapness, high theoretical capacity, ease of synthesis, and environmental friendliness [16,17]. In the same line, we utilized solid solutions of layered Li_2MnO_3 as the cathode material for HSC applications. Iron and nickel containing layered Li_2MnO_3 materials have attracted attention in the recent past as cathodes in lithium batteries, due to their higher capacity, non-toxicity and high operating voltages [18,19]. In this connection, we prepared materials based on a layered manganese oxide solid solution of $Li_{1+x}(Mn_{0.4}Fe_{0.2}Ni_{0.4})_{1-x}O_2$ ($0 < x < 0.4$) with three end members, Li_2MnO_3, $LiNiO_2$ and $LiFeO_2$, using the simple adipic acid assisted sol–gel technique for lithium ion battery applications. Among the composites that were prepared, the material with $x = 0.2$ ($Li_{1.2}(Mn_{0.32}Ni_{0.32}Fe_{0.16})O_2$) at 700 °C showed excellent electrochemical behavior [20].

To the best of our knowledge, the use of such a solid solution as an intercalating type electrode material in HSC applications has not previously been reported. Thus, in the present work, an attempt was made to utilize layered $Li_{1.2}(Mn_{0.32}Ni_{0.32}Fe_{0.16})O_2$ nanoparticles as the electrode for the first time. The HSC is constructed using $Li_{1.2}(Mn_{0.32}Ni_{0.32}Fe_{0.16})O_2$ as the cathode and AC as the anode with 1 M $LiPF_6$ in 1:1 EC/DMC electrolyte solution. The electrochemical performance of the above HSC is evaluated in both potentiostatic and galvanostatic modes between 0 and 3 V at different current densities and the results are presented.

2. Experimental

The conventional sol–gel method was adopted to synthesize $Li_{1.2}(Mn_{0.32}Ni_{0.32}Fe_{0.16})O_2$ with and without a chelating agent (adipic acid, AA). The molar ratio of adipic acid to total metal ions was fixed at 0.25 M. Stoichiometric amounts of $Li(CH_3COO)_2{\cdot}H_2O$ (Wako, Japan), $Fe(CH_3COO)_2{\cdot}H_2O$ (Aldrich, USA), $Ni(CH_3COO)_2{\cdot}4H_2O$ (Aldrich, USA), and $Mn(CH_3COO)_2{\cdot}4H_2O$ (Aldrich, USA) were dissolved separately in distilled water and added to a continuously stirred 0.25 M aqueous solution of adipic acid ($C_6H_{10}O_4$, Sigma–Aldrich, USA). The pH of the solution was maintained at seven using ammonium hydroxide (NH_4OH). The resultant solution was evaporated at 70–80 °C until a transparent sol was obtained and subsequently the water was evaporated. Then, the sol turned into a highly viscous transparent gel. The gel precursors were decomposed at 400 °C for 4 h in air to eliminate the organic moieties. The decomposed powders were ground, pressed into pellets and then sintered at 700 °C for 10 h in an oxygen atmosphere to obtain nano crystalline powders.

The structural and morphological properties of the synthesized nano powders were characterized by X-ray diffraction analysis using Cu Kα radiation (XRD, Rint 1000 Rigaku, Japan) and scanning electron microscopy (S-4700 microscope, Hitachi, Japan), respectively. A Micromeritics ASAP 2010 surface analyzer (Micromeritics, USA) was used to analyze the Brunauer–Emmett–Teller (BET) surface area of the prepared powders. The residual carbon content in the powders was examined by elemental analysis (Elementar Analysen systeme GmbH, Germany).

The electrochemical measurements of the individual electrodes were analyzed by means of a 2032 coin cell configuration where AC or AA-LMNFO was used as working electrode and lithium foil served as counter electrode separated by porous polypropylene film (Celgard 3401, USA). The electrodes for half cells were prepared by pressing a slurry of 80% active material (AC or AA-LMNFO), 10% ketzen black (KB) as conductive additive and 10% Teflonized acetylene black (TAB) as the binder on a 200 mm^2 nickel mesh and dried at 160 °C for 4 h in an oven. The half cells were assembled in an argon filled glove box by pressing a working electrode and lithium counter electrode separated by a separator. The 1 M $LiPF_6$ in a mixture of ethylene carbonate (EC) and dimethyl carbonate (DMC) (1:1 v/v, Soulbrain Co., Ltd, Korea) was used as electrolyte solution. The same procedure was adopted for HSCs construction with LMNFO or AA-LMNFO as cathode and AC anode after optimized the mass ratio of the electrode materials. Cyclic voltammetry and electrochemical impedance spectroscopy studies were performed using an electrochemical analyzer (SP-150, Bio-Logic, France) in a two electrode configuration. Galvanostatic charge/discharge studies were carried out between 0 and 3 V at different current densities using a battery tester (WBCS 3000, Won-A-Tech, Korea). The specific discharge capacitance, average internal resistance and columbic efficiency values of the HSCs were calculated using the formulas described elsewhere [16,17].

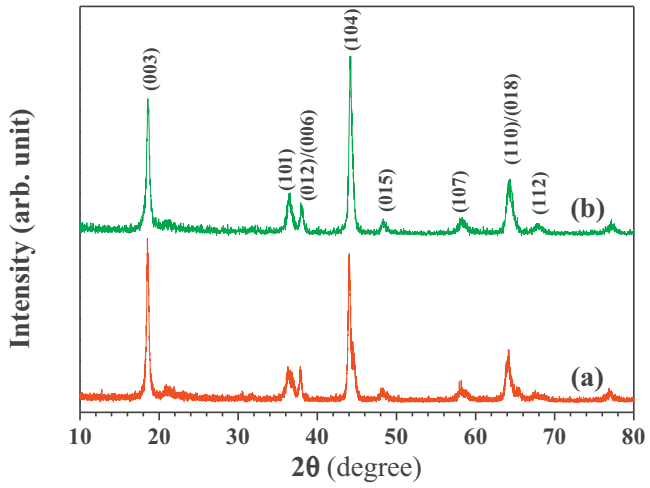

Fig. 1. X-ray diffraction patterns of $Li_{1.2}(Mn_{0.32}Ni_{0.32}Fe_{0.16})O_2$ nanoparticles with chelating agent (a) and without (b) chelating agent.

3. Results and discussion

Fig. 1 shows the XRD patterns of LMNFO and AA-LMNFO prepared at 700 °C for 10 h in an oxygen environment. No impurity phases such as Li_2CO_3, $LiMnO_2$, NiO and α-$LiFeO_2$ are observed in the reflections. The observed peaks are indexed based on the hexagonal α-$NaFeO_2$ structure with space group R-3*m*, which indicates that a layer of lithium atoms is substituted by a layer containing lithium, manganese, nickel and iron atoms [19]. In addition, two small unindexed peaks between 20° and 30° are also noted in Fig. 1, which originate from the short range ordering of the Li, Ni, Mn and Fe atoms in the 3*a* sites, indicating a layered structure with Li_2MnO_3 character [21]. The lattice parameters a_h, c_h and c/a values for LMNFO and AA-LMNFO are calculated and summarized in Table 1. The values are very close to each other and also in good agreement with the reported values [18–21].

Fig. 2 presents the SEM images of the pristine and AA-LMNFO powders. Clear differences could be seen in the particle size and distribution of the LMNFO particulates. Many large and uneven size particles are observed in the LMNFO powders, whereas uniform spherical size particles (~125 nm) with weak aggregation are noted for AA-LMNFO. A BET surface area analysis was performed and it was found that the AA-LMNFO powders showed an average specific surface area of 4.73 $m^2\ g^{-1}$, which is slightly higher than that of the LMNFO powders (4.44 $m^2\ g^{-1}$). This clearly indicates the role of the

Table 1
Lattice parameters and surface areas of LMNFO and AA-LMNFO samples.

Sample	a_h (nm)	c_h (nm)	c/a	Surface area ($m^2\ g^{-1}$)
LMNFO	2.891	14.289	4.951	4.44
AA-LMNFO	2.886	14.285	4.949	4.73

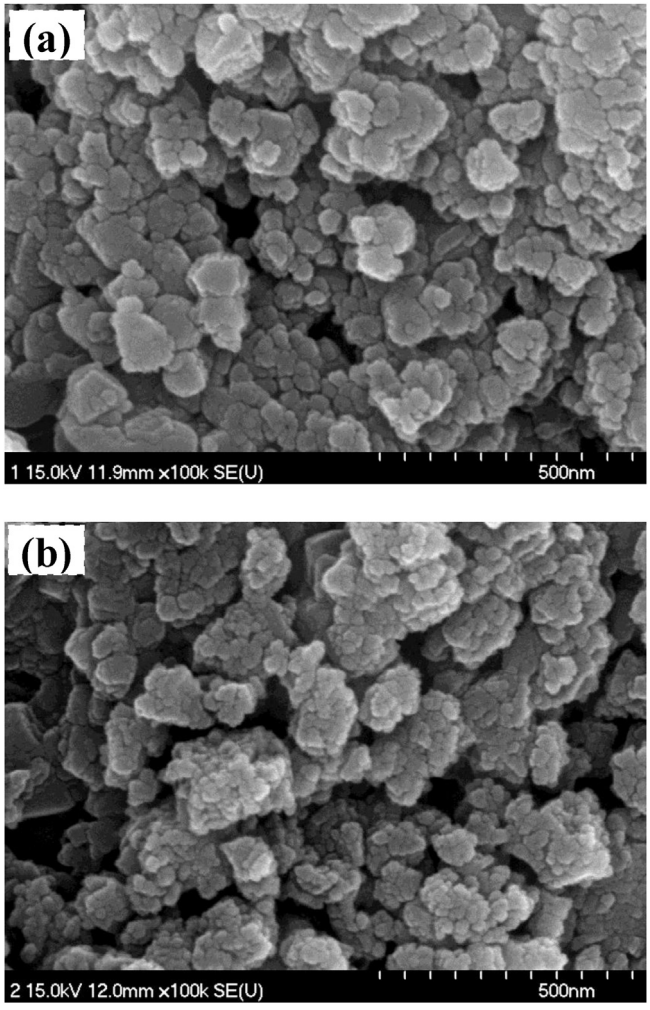

Fig. 2. SEM images of $Li_{1.2}(Mn_{0.32}Ni_{0.32}Fe_{0.16})O_2$ nanoparticles with (a) and without (b) chelating agent.

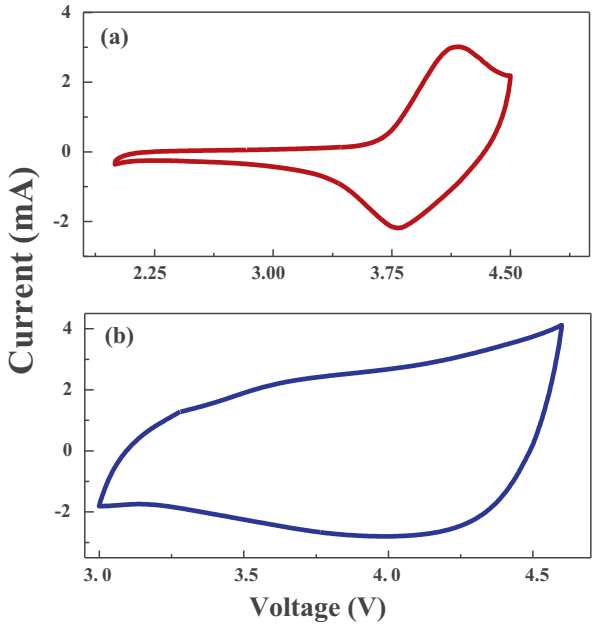

Fig. 3. CV traces of (a) Li^+/AA-LMNFO cell at 0.2 mV s^{-1} scan rate and (b) Li^+/AC cell at 5 mV s^{-1} scan rate recorded between 2–4.5 and 3–4.6 V, respectively.

chelating agent during the solution phase reaction. The purpose of using a chelating agent, particularly carboxylic (—COOH—) functional group containing materials, for example carboxylic acids, is to prevent aggregation during synthesis, but nevertheless some aggregation could still be seen in the SEM pictures. Moreover, during high temperature sintering, adipic acid not only acts as a chelating agent, but also provides the heat of combustion required for the preparation of high crystalline nano powders with a relatively large surface area [22]. It can be concluded from the SEM and BET studies that the chelating agent played a major role during calcination, leading to a reduction of the particle size with an accompanying increase in the specific surface area of the materials. It is believed that smaller size particles with a high surface area are better for lithium ions, because they reduce the pathways for their diffusion during the electrochemical reaction, enabling faster electronic transport through the size effect.

3.1. Electrochemical performance of the half cells

In order to investigate the individual performance of AA-LMNFO and AC electrodes, CV studies were carried out in 1 M $LiPF_6$ (EC:DMC, 1:1 v/v) electrolyte at ambient temperature. Fig. 3 presents the CV curves of Li/AA-LMNFO and Li/AC cells recorded at 0.2 and 5 mV s^{-1}, respectively, between 0 and 3 V against lithium counter electrode. As seen from Fig. 3, CV traces of two individual electrodes have exhibited different electrochemical behavior. In the case of Li/AA-LMNFO cell, there is an appearance of one anodic peak around at ~4.2 V during charging process and corresponding reduction peak is observed at ~3.6 V on discharge process. These peaks are attributed to the redox reaction of Ni^{2+}/Ni^{4+} couple as was speculated elsewhere [18,20]. Furthermore, the absence of redox peak ~3 V suggested that Mn ions are electrochemically inactive and are presented in Mn^{4+} state in all samples [20]. In addition, no transition of $Fe^{3+/4+}$ is observed at around 4 V throughout the region tested as shown in Fig. 3a, which clearly revealing that Mn and Fe are electrochemically inactive and are mostly acted as activator to stabilize LMNFO structure during the electrochemical reaction. On the other hand, the CV traces of Li^+/AC cell (Fig. 3b) measured at 5 mV s^{-1} showed a typical double layer capacitive behavior (i.e. rectangular shape) between 3 and 4.6 V. It is worthy to mention here that AA-LMNFO could be used as high performance electrode material for HSC application along with AC anode when compared to commercialized pre-lithiated graphitic electrode (G)/AC configuration. It is well known that the pre-lithiation of graphite leads to the large volume expansion and pulverize the electrode during the charge discharge process, which affected the electrochemical reversibility and thereby decreasing the overall cyclic behavior of G/AC system [23]. In contrast, the Mn and Fe activators in AA-LMNFO material stabilized its structure and increasing the electrochemical stability of AA-LMNFO/AC hybrid cell during charge–discharge cycles.

It is well known that the capacitive nature of supercapacitors was strongly related to the weight ratio of individual electrode. Generally, the symmetrical capacitors were constructed based on same kind of electrodes with same mass loading experiences same reaction mechanism in which the applied voltage was shared equally between the electrodes. In the case of capacitor fabricated with different electrodes with different storage mechanism, the applied voltage will split based on the capacitive performance of each electrode separately. Therefore, a mass balance of individual electrode is required to fabricate high capacitive performance with enhanced cycle life [24]. In the present study, the mass balance of each electrode was optimized from the charge–discharge studies of Li^+/AC and Li^+/AA-LMNFO half cells at 400 mA g^{-1} current density and corresponding curves were illustrated in Fig. 4.

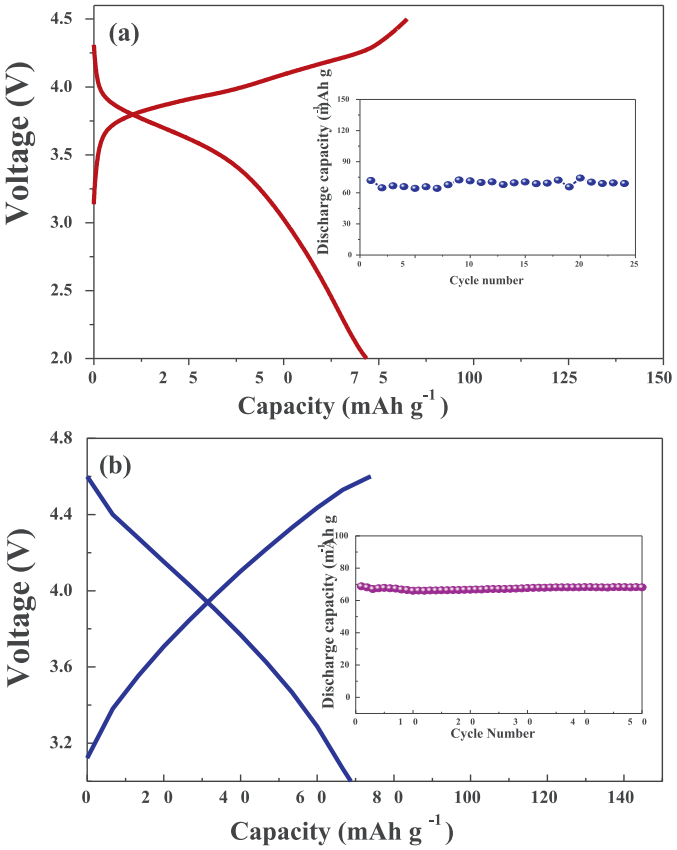

Fig. 4. Charge–discharge curves of (a) The Li^+/AA-LMNFO cell between 2 and 4.5 V and (b) the Li^+/AC cell between 3 and 4.6 V measured at the constant current density of 400 mA g^{-1} in 1 M $LiPF_6$ (EC/DMC, 1:1 v/v) electrolyte. The corresponding cycle performance data are shown as insets.

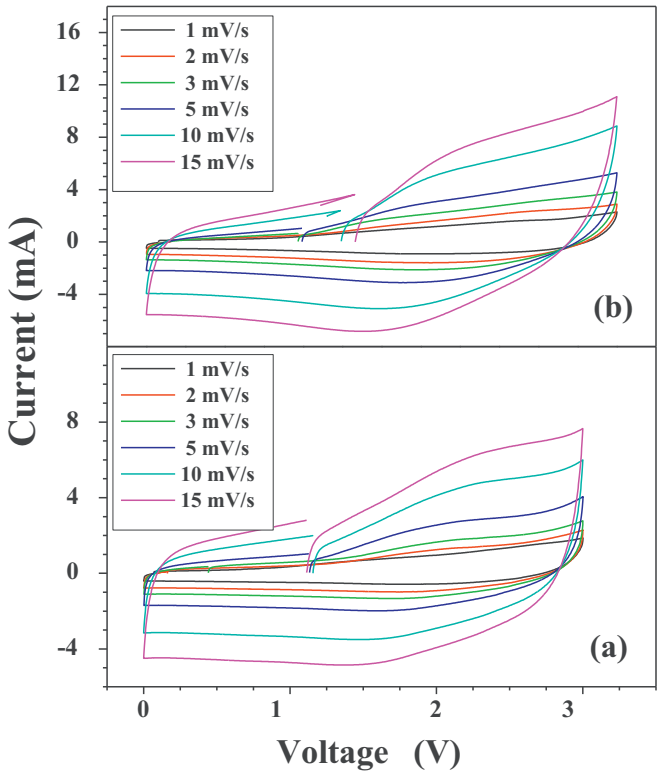

Fig. 5. CV curves of (a) LMNFO/AC cell and (b) AA-LMNFO/AC cell in 1 M $LiPF_6$/1:1 EC/DMC electrolyte with different scan rates.

Since the decomposition of carbonate based electrolyte occurred ~4.6 V against Li^+/Li, the testing potential range for Li^+/AA-LMNFO and Li^+/AC cells were restricted between 2–4.5 and 3–4.6 V, respectively. As seen from Fig. 4a, the Li^+/AA-LMNFO cell showed typical lithium intercalation/deintercalation property between 2 and 4.5 V in 1 M $LiPF_6$ (EC:DMC, 1:1 v/v) electrolyte [ref]. Whereas, the Li^+/AC cell showed typical non-Faradaic storage mechanism (Fig. 4b) along with the adsorption/desorption of PF_6^- anion on the surface of AC electrode, resulting the formation of electrical double layer between the electrode–electrolyte interfaces. As can be seen from Fig. 4, a discharge capacity of about 68 and 72 mAh g^{-1} was obtained for Li^+/AC and Li^+/AA-LMNFO half cells, respectively. In addition, both the cells showed excellent cycleability as shown as inserts in Fig. 4 with prolonged cycles. This prolonged cycling behavior suggested that both AC and AA-LMNFO electrodes were compatible for HSC application in standard inorganic electrolyte. Based on charge–discharge studies of AC and AA-LMNFO vs Li^+/Li at the same current rates, the mass ratio of anode and cathode for HSC construction was optimized as 1:1.05

3.2. Performance evaluation of HSC cells

The electrochemical performance of the HSC was investigated by means of cyclic voltammetry (CV) with a two-electrode coin cell configuration. CV is a universally accepted and appropriate tool for estimating the difference between the Faradic and non-Faradic reactions during an electrochemical reaction [25]. Fig. 5 presents the CV curves of LMNFO/AC and AA-LMNFO/AC HSCs at different sweep rates ranging from 1 to 15 mV s^{-1} between 0 and 3 V. It could be seen that all of the curves showed an almost rectangular mirror-like shape with respect to zero current and a rapid current response on voltage reversal at each end potential. The shapes of the CV curves showed that the current responses depended on the scanning rate. Moreover, all of the curves maintained their mirror image shape even at higher scanning rates, which indicates excellent capacitive behavior with reversibility. Fig. 5b clearly demonstrates that the AA-LMNFO/AC cell exhibits a stronger current response and higher specific capacitance than the LMNFO/AC cell (Fig. 5a). The higher current response of the AA-LMNFO/AC cell might be due to the small particles with highly exposed surface area and good contact with the current collector [26].

The galvanostatic charge–discharge profiles of the LMNFO/AC and AA-LMNFO/AC HSCs were studied in the presence of 1 M $LiPF_6$ in1:1 EC/DMC electrolyte solution between 0 and 3 V and the results are presented in Fig. 6. The HSC cells are charged and discharged at a constant current density of 1 mA cm^{-2} up to 1000 cycles. It is obvious from the cycling curves that the potential varied linearly with time during charge and discharge. This reveals that the hybrid cell exhibits good electrochemical capacitance behavior with excellent reversibility. Although an almost linear potential response is observed, the cycling curves do not have a good triangular shape, which may be due to the combination of the redox reaction process occurring at the cathode, the voltage changes due to ion separation between the electrode/electrolyte interface and the ohmic resistance. These results showed that the hybrid system exhibited both EDLC and battery type behavior. The storage mechanism of LMNFO electrode in LMNFO/AC cell mainly depends on electron transfer and Faradaic reaction of reversible lithium intercalation/deintercalation, which produced pseudocapacitance, ensuring high energy density of the hybrid cell. On the other hand, Li-ions were adsorbed and de-adsorbed on AC electrode surface during the charge–discharge process to maintain the charge neutrality of the electrolyte solution. The adsorbed cations forms the electric double layer, providing necessary power density and Li

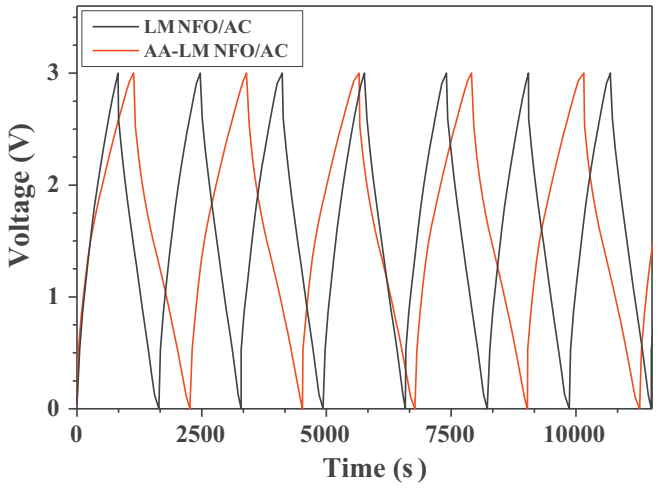

Fig. 6. Typical charge–discharge traces of (a) LMNFO/AC and (b) AA-LMNFO/AC cell between 0 and 3 V at a constant current density of 1 mA cm^{-1}.

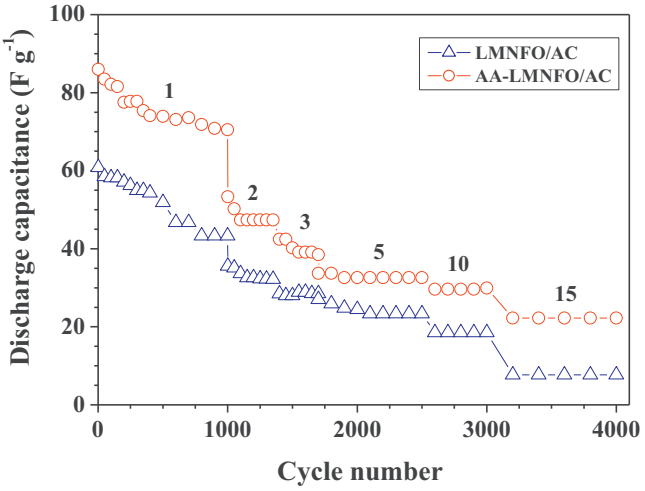

Fig. 7. Ganvanostatic cycling profiles of hybrid supercapacitors recorded between 0 and 3 V with different current densities.

intercalation/deintercalation process of LMNFO provides the high energy density of the HSC. The following equations explain the possible charge storage mechanism of LMNFO/AC cell [17]

$$\text{Cathode}: Li_{1.2}(Mn_{0.32}{}^{4+}Ni_{0.32}{}^{2+}Fe_{0.16}{}^{3+})O_2 \Leftrightarrow Li_{1.2-x}(Mn_{0.32}{}^{4+}Ni_{0.32}{}^{3+}Fe_{0.16}{}^{3+})O_2 + (1+x)Li^+ + xe^-$$

$$\text{Anode}: AC + (1+x)Li^+ + xe^- \Leftrightarrow AC(xe^-) + //(1+x)Li^+ (//\text{stands for double layer})$$

The internal resistances of the LMNFO/AC and AA-LMNFO/AC HSCs were calculated and found to be 45 and 26 Ω, respectively. The specific discharge capacitance of the AA-LMNFO/AC HSC is found to be 86 F g^{-1} at a current density of 1 mA cm^{-2} and retained about 87% of this value after 1000 cycles. On the other hand, the LMNFO/AC cell delivered initial discharge specific capacitances of 61 and 43 F g^{-1} at the first and 1000th cycles, respectively, which corresponds to 70% capacity retention. However, the columbic efficiency of both HSCs was over 99% even after 1000 cycles. Usually, the cycle life of an electrode mainly depends on the operating rate and depth-of-discharge, which determine the deliverable energy and power density [25].

Fig. 7 illustrates the cycling performance of the HSCs at different current densities recorded at room temperature. The HSCs were initially cycled at a constant current density of 1 mA cm^{-2} for 1000 cycles and continuously employed at various current densities from 2 to 15 mA cm^{-2}. As expected, the specific discharge capacitances of both the LMNFO/AC and AA-LMNFO/AC HSCs decreased with increasing current density. The variations in the discharge capacitance can be attributed to the large ohmic drop, which leads to small capacitance values, and also to the polarization effects at higher current densities, which result in the low utilization of the active materials [27]. In particular, the lithium ions do not have enough time to intercalate into the crystal lattice and, thus, the electrochemical reaction takes place only on the surface of the active particles, causing reduction in the discharge capacitance values at high current densities [28].

Fig. 8 represents the Ragone plot and plot of the discharge capacitance vs. current density for both HSCs. From Fig. 8a, it is evident that the AA-LMNFO/AC HSC exhibited excellent rate performance with improved electrochemical behavior even at high current rates compared to the LMNFO/AC. The specific power (P, W kg^{-1}) and specific energy (E, Wh kg^{-1}) densities of the HSCs were calculated using the following formula and the results obtained are presented in Fig. 8b as a Ragone plot.

$$P = \frac{I\Delta E}{m}$$

$$\Delta E = \frac{E_{max} + E_{min}}{2}$$

$$E = P^{\bullet}t$$

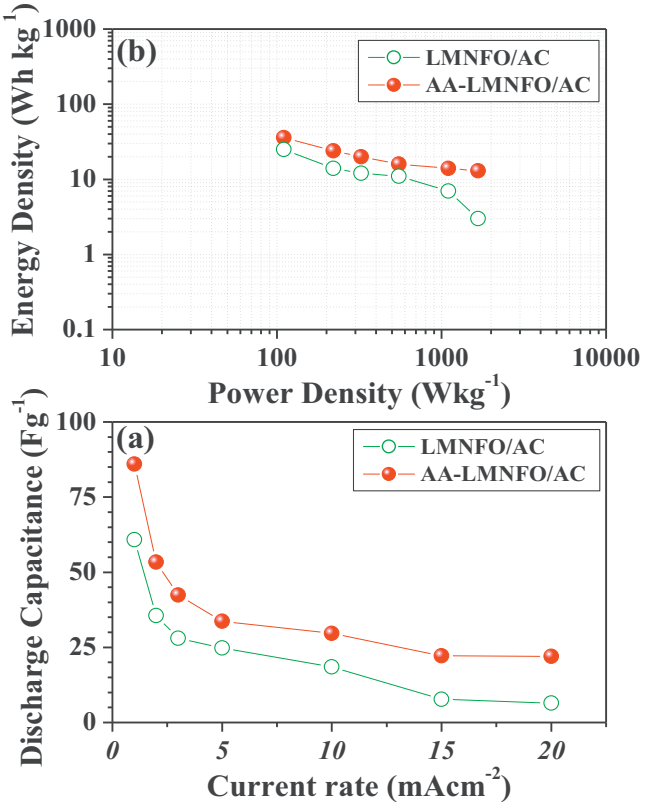

Fig. 8. (a) Plots of specific discharge capacitance vs. current density and (b) Ragone plot of HSCs.

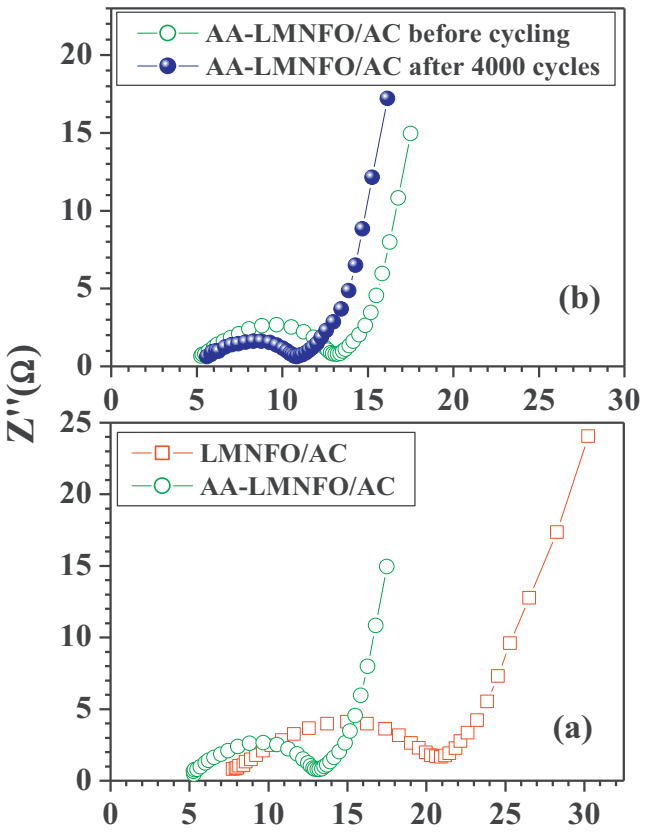

Fig. 9. Nyquist plots of HSCs: (a) EIS spectra of freshly made LMNFO/AC and AA-LMNFO/AC cells under open circuit voltage conditions, (b) EIS spectra of AA-LMNFO/AC cells before and after 4000 cycles.

where I is the current density, E_{max} and E_{min} are the potentials at the beginning of discharge and the end of discharge, respectively, m is the weight of active material and C is the capacitance of the HSC. The Ragone plot clearly demonstrated that the AA-LMNFO/AC hybrid capacitor is capable of delivering higher energy densities than the LMNFO/AC cell, for instance, the AA-LMNFO/AC cell delivered maximum specific energy and power densities of 36 Wh kg^{-1} and 1.67 kW kg^{-1}, respectively. This improved electrochemical performance of the AA-LMNFO/AC HSC is attributed to the better structural properties along with relatively larger surface area and small size of the particle, which facilitates the electron transport at high current rates. Fig. 9 illustrates the family of Nyquist plots for the LMNFO/AC and AA-LMNFO/AC HSCs before and after cycling recorded in the frequency range of 100 kHz–100 mHz under open circuit voltage conditions. Fig. 9a shows the EIS spectra of the freshly made cells and both curves consist of a semicircle in the high frequency region, followed by a straight line in the low frequency region. The semicircle part in the high frequency region represents the charge transfer resistance (R_{ct}), which is also known as the faradaic resistance at the electrode–electrolyte interface. The straight line inclined at 45° to the real axis corresponds to the diffusion of ions in the LMNFO electrodes. It can be seen from the Nyquist plots that the AA-LMNFO/AC showed a lower R_{ct} value (~7.7 Ω), which is almost half of that of its counterpart LMNFO/AC (~14.2 Ω). The variation of the R_{ct} values was expected, since the addition of a chelating agent during synthesis would increase the specific surface area by reducing the particle size, thereby improving the sluggish kinetic behavior of the intercalating type electrodes, which would certainly increase the electrochemical performance of the HSCs. Fig. 9b represents the EIS spectra of the AA-LMNFO/AC HSC before and after 4000 cycles. It is obvious that the diameter of the semicircle, as well as the R_{ct} values, is slightly decreased after 4000 cycles. This behavior may be ascribed to the increase in the electrode area due to the expansion and contraction processes during cycling. The lowering of the resistance value increases the current density on the electrode surface and, hence, significantly increases the rate capability and cycle performance, and the galvanostatic cycling profiles are well correlated with this behavior. Moreover, the straight line in the low frequency range is inclined at an angle of approximately 90° to the real axis after 4000 cycles, indicating that the AA-LMNFO/AC cell exhibits excellent capacitive behavior in a non-aqueous medium such as 1 M $LiPF_6$ in 1:1 EC/DMC solution.

4. Conclusion

Low cost, nanoscale $Li_{1.2}(Mn_{0.32}Ni_{0.32}Fe_{0.16})O_2$ powders were synthesized by the sol–gel technique with and without a chelating agent. The prepared $Li_{1.2}(Mn_{0.32}Ni_{0.32}Fe_{0.16})O_2$ nanoparticles exhibited a layered α-$NaFeO_2$ structure. A hybrid supercapacitor was constructed with activated carbon to evaluate the supercapacitive behavior with 1 M $LiPF_6$ in 1:1 EC/DMC electrolyte solution between 0 and 3 V at room temperature. The results revealed that the $Li_{1.2}(Mn_{0.32}Ni_{0.32}Fe_{0.16})O_2$ nanoparticles prepared with a chelating agent exhibited better capacitive properties with over 87% capacity retention after 1000 cycles. The HSC delivered maximum energy and power densities of 36 Wh kg^{-1} and 1.67 kW kg^{-1}, respectively, at room temperature. These results indicate that the $Li_{1.2}(Mn_{0.32}Ni_{0.32}Fe_{0.16})O_2$ nanoparticles prepared with a chelating agent could be used as a promising electrode material for hybrid supercapacitor applications in the near future.

Acknowledgement

This study was support from IT R&D program of MKE/KEIT. [KI10039182, Development of 5 V cathode material which capacity is 125 mAh g^{-1} & high voltage electrolyte which decomposition is over 5 V for lithium secondary battery].

References

[1] B.E. Conway, Transition from supercapacitor to battery behavior in electrochemical energy storage, Journal of the Electrochemical Society 138 (1991) 1539.
[2] M. Winter, R.J. Brodd, What are batteries, fuel cells, and supercapacitors? Chemical Reviews 104 (2004) 4245.
[3] T. Brousse, M. Toupin, D. Belanger, A hybrid activated carbon-manganese dioxide capacitor using a mild aqueous electrolyte, Journal of the Electrochemical Society 151 (2004) A614.
[4] M. Nakamura, M. Nakanishi, K. Yamamoto, Influence of physical properties of activated carbons on characteristics of electric double-layer capacitors, Journal of Power Sources 60 (1996) 225.
[5] R. Kotz, M. Carlen, Principles and applications of electrochemical capacitors, Electrochimica Acta 45 (2000) 2483.
[6] P. Simon, Y. Gogosti, Materials for electrochemical capacitors, Nature Materials 7 (2008) 845.
[7] A.S. Arico, P.G. Bruce, B. Scrosati, J.M. Tarascon, W.V. Schalkwijk, Nanostructured materials for advanced energy conversion and storage devices, Nature Materials 4 (2005) 366.
[8] F. Chen, R.G. Li, M. Hou, L. Liu, R. Wang, Z.H. Deng, Preparation and characterization of ramsdellite $Li_2Ti_3O_7$ as an anode material for asymmetric supercapacitors, Electrochimica Acta 51 (2005) 61.
[9] A.D. Pasquier, A. Laforgue, P. Simon, $Li_4Ti_5O_{12}$/poly(methyl)thiopheneasymmetric hybrid electrochemical device, Journal of Power Sources 125 (2004) 95.
[10] Y.G. Wang, Y.Y. Xia, A new concept hybrid electrochemical surpercapacitor: carbon/$LiMn_2O_4$ aqueous system, Electrochemistry Communications 7 (2005) 1138.
[11] Y. Zhao, Y.Y. Wang, Q.Y. Lai, L.M. Chen, Y.J. Hao, X.Y. Ji, Pseudocapacitance properties of AC/$LiNi_{1/3}Co_{1/3}Mn_{1/3}O_2$ asymmetric supercapacitor in aqueous electrolyte, Synthetic Metals 159 (2009) 331.
[12] Y.J. Hao, Q.Y. Lai, X.Y. Xu, L. Wang, Electrochemical performance of symmetric supercapacitor based on $Li_4Mn_5O_{12}$ electrode in Li_2SO_4 electrolyte, Materials Chemistry and Physics 126 (2011) 432.
[13] S.H. Choi, J. Kim, Y.S. Yoon, Fabrication and characterization of a $LiCoO_2$ battery–supercapacitor combination for a high-pulse power system, Journal of Power Sources 138 (2004) 360.

[14] H. Kawai, M. Ngata, H. Tsukamoto, A.R. West, A new lithium cathode $LiCoMnO_4$: toward practical 5 V lithium batteries, Electrochemical and Solid-State Letters 1 (1998) 212.
[15] H. Wu, C.V. Rao, B. Rambabu, Electrochemical performance of $LiNi_{0.5}Mn_{1.5}O_4$ prepared by improved solid state method as cathode in hybrid supercapacitor, Materials Chemistry and Physics 116 (2009) 532.
[16] K. Karthikeyan, V. Aravindan, S.B. Lee, I.C. Jang, H.H. Lim, G.J. Park, M. Yoshio, Y.S. Lee, Electrochemical performance of carbon-coated lithium manganese silicate for asymmetric hybrid supercapacitors, Journal of Power Sources 195 (2010) 3761.
[17] K. Karthikeyan, V. Aravindan, S.B. Lee, I.C. Jang, H.H. Lim, G.J. Park, M. Yoshio, Y.S. Lee, A novel asymmetric hybrid supercapacitor based on Li_2FeSiO_4 and activated carbon electrodes, Journal of Alloys and Compounds 504 (2009) 224.
[18] M. Tabuchi, Y. Nabeshima, K. Ado, M. Shikano, H. Kageyama, K. Tatsumi, Material design concept for Fe-substituted Li_2MnO_3-based positive electrodes, Journal of Power Sources 174 (2007) 554.
[19] M. Tabuchi, Y. Nabeshima, T. Takeuchi, H. Kageyama, K. Tatsumi, J. Akimoto, H. Shibuya, J. Imaizumi, Synthesis and electrochemical characterization of Fe and Ni substituted Li_2MnO_3-an effective means to use Fe for constructing Co-free Li_2MnO_3 based positive electrode material, Journal of Power Sources 196 (2011) 3611.
[20] K. Karthikeyan, S. Amaresh, G.W. Lee, V. Aravindan, H. Kim, K.S. Kang, Y.S. Lee, Electrochemical performance of cobalt free, $Li_{1.2}(Mn_{0.32}Ni_{0.32}Fe_{0.16})O_2$ cathodes for lithium batteries, Electrochimica Acta 68 (2012) 246.
[21] Y. Sun, C. Ouyang, Z. Wang, X. Huang, L. Chen, Effect of Co content on rate performance of $LiMn_{0.5-x}Co_{2x}Ni_{0.5-x}O_2$ cathode materials for lithium-ion batteries, Journal of The Electrochemical Society 151 (2004) A504.
[22] Y.S. Lee, Y.K. Sun, K.S. Nahm, Synthesis of spinel $LiMn_2O_4$ cathode material prepared by an adipic acid-assisted sol–gel method for lithium secondary batteries, Solid State Ionics 109 (1998) 285.
[23] S.R. Sivakkumar, A.G. Pandolfo, Evaluation of lithium-ion capacitors assembled with pre-lithiated graphite anode and activated carbon cathode, Electrochimica Acta 65 (2012) 280.
[24] K. Karthikeyan, S. Amaresh, K.J. Kim, S.H. Kim, K.Y. Chung, B.W. Cho, Y.S. Lee, A high performance hybrid capacitor with Li_2CoPO_4F cathode and activated carbon anode, Nanoscale 5 (2013) 5958.
[25] Q. Wang, Z. Wen, J. Li, A hybrid supercapacitor fabricated with a carbon nanotube cathode and a TiO_2-B nanowire anode, Advanced Functional Materials 16 (2006) 2141.
[26] S. Alvarez, L.M.C. Blanco, O.A.J. Miranda, A.B. Fuertes, T.A. Centeno, Electrochemical capacitor performance of mesoporous carbons obtained by templating technique, Carbon 43 (2005) 866.
[27] K. Zaghib, J.B. Goodenough, A. Mauger, C. Julien, Unsupported claims of ultra-fast charging of $LiFePO_4$ Li-ion batteries, Journal of Power Sources 194 (2009) 1021.
[28] X.M. Wu, X.H. Li, Z. Wang, Z.B. Xiao, J. Liu, W.B. Yan, Characterization of solution-derived $LiMn_2O_4$ thin films heat-treated by rapid thermal annealing, Materials Chemistry and Physics 83 (2004) 78.